Distinguishing between Structural Models of β'-sialons using a Combined Solid-State NMR, Powder XRD and Computational Approach

V. R. Seymour[1,2] and M. E. Smith[1,3]*

1. Department of Chemistry, Lancaster University, Bailrigg, Lancaster, LA1 4YB, UK

2. Materials Science Institute, Lancaster University, Bailrigg, Lancaster, LA1 4YB, UK

3. Vice-Chancellor's Office, University House, Lancaster University, Bailrigg, Lancaster, LA1 4YW, UK.

Abstract

β'-sialons ($Si_{6-z}Al_zO_zN_{8-z}$, where $0 \leq z \leq \sim 4.2$) are studied using a combination of ^{29}Si and ^{27}Al solid-state NMR, including using magnetic fields of up to 20 T, powder X-ray diffraction and Density Functional Theory (DFT) calculations of both the structure and NMR parameters. Four different structural models have been proposed in the literature for the replacement of silicon and nitrogen by aluminium and oxygen within a β-Si_3N_4-structured lattice. Experimental data is presented of the variation with composition (z) of the unit cell parameters from diffraction and the local coordination units present suggested by NMR data. The experimental data is compared to the changes with composition in the DFT calculations of the structure and the NMR parameters according to the four models, allowing the models to be distinguished. It is shown that only one of these, the domain model is fully consistent with all of the experimental data and is therefore a good structural model for β'-sialons. More speculatively it is suggested that for the domain model, ^{27}Al NMR data might provide a constraint on the thickness of its aluminium-rich layers.

Corresponding author

*Mark E. Smith, Vice-Chancellor's Office, Lancaster University, Bailrigg, Lancaster, LA1 4YW, UK.

Email: m.e.smith@lancaster.ac.uk

Introduction

Silicon aluminium oxynitride (sialon) ceramics have generated much interest as they can possess attractive combinations of thermal and mechanical properties, as well as high chemical inertness.[1-3] Sialons based on the β-silicon nitride (Si_3N_4) structure (Figure 1a)[4] (termed β'-sialon) show a significant compositional range with the general formula $Si_{6-z}Al_zO_zN_{8-z}$, where $0 \leq z \leq \sim 4.2$.[3] In such materials aluminium substitutes for silicon while concomitantly oxygen does so for nitrogen.[5] That β'-sialon occurs over such an extensive compositional range is due to the close match of the Si-N and Al-O bond lengths, maintaining the β-Si_3N_4 structure, with the lattice parameters increasing with z.[6] However, this then implies that full stochastic atomic mixing is unlikely and some type of local ordering/clustering occurs to maximise the number of Si-N and Al-O bonds. A detailed understanding of the atomic ordering is of real fundamental structural chemistry interest, and has recently become practically and technologically much more important as sialons have started to be used in more functional applications, for example doped with relevant ions to produce efficient phosphor materials.[7-10] For such applications the crystal structure of the host material, in particular the local coordination around the luminescence centres plays a crucial role.

XRD data for β'-sialons provides the unit cell parameters, but only very limited information on the relative distributions of Al/Si and O/N. Neutron diffraction provides better relative elemental contrast, with several such studies of β'-sialons reported.[6,11,12] The literature X-ray and neutron diffraction data used here is summarised in Table S1 in the supporting information (SI). The neutron data provides average occupancies over the structure for each site and this is indicated by the fractional occupancies indicated in Figure S1. However, the structurally interesting question concerns not the average occupancies, but the detail of the distribution of the $(Si,Al)O_xN_{4-x}$ ($0 \leq x \leq 4$) tetrahedra that make up the structure (Figure 1b). Other experimental methodologies have been applied to look at atomic ordering within β'-sialons, including Al-K and Si-K edges extended X-ray absorption fine structure (EXAFS) which reinforced the suggestion of the preference of Si-N and Al-O bonds in the structure, with only a relatively narrow range of the bond lengths observed as the composition changed.[13] An Si-N/Al-O preference is further confirmed by X-ray photoemission spectroscopy (XPS)[14] and X-ray absorption near-edge structure (XANES)[15] studies. This X-ray spectroscopy data[13-15] provides some underlying understanding of the average distribution of the elements within the structure. The models suggested here take into account, and are

consistent with all of these previous measurements, but better constrain the distribution of local units present by comparing the NMR data to the distribution of the units predicted by different structural models. Previous solid-state NMR also has already suggested a Si-N and Al-O bonding preference[16-18] confirmed by these X-ray measurements. The potential advantage of NMR to accurately quantify *all* the different local environments present has not been fully exploited in earlier work (more details *vide infra*).

With recent advances in computational chemistry the structural models for β'-sialon have been re-examined by calculating the changes in structure, to give both the lattice parameters and NMR interaction parameters. Structural models suggested for β'-sialon include (i) a layered domain model based on the observations of the original NMR work[16,17], (ii) a channel model[19,20] and (iii) a plane model[21] (see Figure 1c, with the unit cells and local environments created using Vesta[22]). The different models and their atomic distributions are shown in detail in Figures S2 and S3. All show the required predominance of Si-N and Al-O bonds. However, a detailed inspection of the range of local coordination units present and change in their relative abundance with composition for each model has not been carried out. For completeness the distribution of local coordination units under (iv) a random distribution of the elements is also compared here, although DFT is not applied to this model. DFT computational approaches have been previously applied to understand the atomic ordering within β'-sialons.[23,24] Boyko *et al.* recently used DFT to compare the NMR and channel (Okatov) models, concluding that the latter better reproduced the experimental measurements. It should be noted that this conclusion is based on the calculated band gap which is a single constraint, collapsing all of the rich structural data into a single parameter.[25]

NMR is an excellent probe for distinguishing local environments, providing the complete distribution rather than an 'average' environment. As magic angle spinning (MAS) started to be applied to inorganic solids[26] different local tetrahedral silicon environments (Q^n) were distinguished on the basis of their different chemical shifts.[26,27] ^{27}Al similarly developed into a key probe nucleus of some inorganic materials where the peak position could often distinguish the local coordinations AlO_4, AlO_5 and AlO_6.[26-30] The spectra from ^{27}Al are more complicated to interpret than for ^{29}Si because of the additional presence of the quadrupolar interaction.[31] Oxynitride phases provided a great expansion of the local aluminium and silicon coordination environments studied by NMR from the earlier work on silicates and aluminosilicates where oxygen dominated the local coordination units. The early MAS NMR

work on oxynitride ceramics is summarised in ref. 32. Most initial NMR observations were from crystalline oxynitrides with only a small number of well-defined local sites present in the structure. ^{29}Si MAS NMR was usually able to distinguish different local environments SiO_xN_{4-x} ($0 \leq x \leq 4$) from the isotropic chemical shift.[33,34] For ^{27}Al, early NMR from oxynitrides showed changes in peak positions attributed to changes of x in AlO_xN_{4-x}. However, with the relatively low magnetic fields then available, residual second-order quadrupolar broadening under MAS caused significant overlap of the different peaks meaning clear cut resolution and accurate quantification was not possible.[16,17] Previous solid-state NMR data from β-Si_3N_4 and β'-sialons is summarised in Table S2.[16-18,35-39]

Since the initial NMR reports on β'-sialons there have been very significant advances in solid-state NMR instrumentation and methodology.[40] A recent study used the latest ultrahigh field solid-state NMR along with DFT calculations of NMR parameters to investigate the very low z end of the β'-sialon range (i.e., z = 0.050-0.125).[18] Although that study well illustrated the very strong tendency for Al-O bond formation, even at low oxygen concentrations, it did not look to distinguish between the more detailed structural models that have been proposed. It would have been difficult in that study to go further than simply ruling out a random distribution given the limited z-range investigated. This current study uses a range of applied magnetic fields up to 20 T with fast MAS and two-dimensional (2D) multiple-quantum (MQ) MAS NMR techniques[41,42] across effectively the complete z-range for β'-sialons to test which of the structural models provides the most appropriate description of the local ordering. Periodic DFT-based methods are used to calculate the NMR parameters together with the distribution of the different units in each proposed model structure. The variation and distribution in the NMR parameters are combined with the changes in the lattice parameters with z to differentiate the proposed structural models.

Experimental Methods

Samples and Phase Identification

The samples of β'-sialon (z = 1, 2, 4) studied here are exactly the same ones as reported previously[16,17,35] prepared by hot pressing of oxide and nitride components. To confirm the phase identification laboratory powder X-ray diffraction (PXRD) of the samples was performed on a Rigaku SmartLab instrument, using a 9 kW Cu-source generator. Typically, 5° to 90° 2θ ranges were investigated over ~20 mins, with a step size of 0.01°. The XRD patterns

are shown in Figure S4. The samples are confirmed as phase pure apart from the z = 4 sample where some additional minor peaks can be seen.

Solid-State NMR

^{27}Al one-dimensional (1D) MAS and two-dimensional (2D) MQMAS NMR spectra were obtained at 16.4 and 20.0 T, at Lancaster University and at the UK 850 MHz solid-state NMR Facility, respectively. At 16.4 T, powdered samples were packed into 2.5 mm MAS rotors, and rotated at MAS rates of 30 kHz. 1D ^{27}Al NMR spectra were recorded using a short flip angle of 0.7 μs, with signal averaging for 696 to 800 transients, and a recycle delay of 5 s. At 20.0 T, 2.5 mm MAS rotors were used, and rotated at MAS rates of 25 kHz. 1D ^{27}Al spectra were recorded using a Hahn echo pulse sequence, with rf of ~76 kHz and an echo spacing of ~30-40 μs. Signal averaging by co-adding 256 to 2048 transients, and a recycle time of 0.5 s was used. At longer recycle times no significant differences were observed. 2D ^{27}Al spectra were recorded using a shifted-echo split-t_1 3Q MAS pulse sequence with the signal enhanced using a SPAM composite conversion pulse.[43,44] 2D spectra were recorded with signal averaging for 256 to 5376 transients for each of 28 to 48 t_1 increments of 51.67 μs. The spectra were referenced in the indirect dimension according to Ref. 45. A recycle delay of 0.25 s was used. ^{29}Si 1D MAS NMR spectra were obtained at 16.4 T, using a standard single pulse sequence, with a 4 mm HX probe and a 30° tip angle pulse, signal averaging 8 to 24 transients, with a recycle time of 1800 s. NMR spectra were calibrated using secondary, solid standards of $Al(acac)_3$ for ^{27}Al (δ_{iso} = 0 ppm, C_Q = 3.0 MHz, η_Q = 0.15) and kaolinite for ^{29}Si (δ_{iso} = −91.2 ppm).

DFT Computational Work

To aid understanding of the experimental NMR spectra, NMR parameters were calculated for the different models of β'-sialon. Calculations of NMR parameters were carried out using the CASTEP code (8.0 Academic Release)[46-49] on Lancaster University's High End Computer cluster. A plane-wave energy cut-off of 50 Ry (~680 eV) was used, and integrals over the Brillouin zone were performed using a k-point spacing of 0.05 2π Å^{-1}. Convergence tests of the total energy and calculated NMR parameters with respect to the energy cut-off and k-point spacing were carried out. Reference shielding values (σ_{ref}) of 556.8 and 328.88 ppm were used for ^{27}Al and ^{29}Si, respectively (see SI (Section S4) for further detail). Structural

parameters, atomic coordinates and unit cell parameters were obtained from experimental crystal structures in the literature.[9] Prior to the calculation of NMR parameters, geometry optimisation of the models was performed by allowing both the atomic coordinates and unit cell to relax.

Results and Discussion

Experimental NMR Data

^{29}Si MAS NMR spectra for each sample showed a single peak at approximately −48 ppm, which is similar to β-Si_3N_4 (SiN_4) (See SI Figure S6). As noted, previously[35], a small increase in linewidth is observed, with increasing substitution (linewidths from 2.3-4.7 ppm, Table 1).

z	Expt. ^{29}Si NMR parameters		DFT (CASTEP)	
	Peak maxima (ppm)	Full width at half max. (ppm)	Model (see SI for details of the nomenclature)	^{29}Si δ_{iso} range (ppm)
1	−48.4 (0.1)	2.3 (0.3)	channel 231 domain 113 domain 116	3.3 3.0 2.5
2	−48.2 (0.1)	3.3 (0.4)	channel 231 channel 331 plane 221 domain 113 domain 116	3.8 0.9 11.5 3.2 5.2
4	−47.0 (0.4)	4.7 (0.5)	channel 231 channel 331 plane 221 domain 113 domain 116i domain 116ii	4.8 0.0 0.3 4.4 2.6 2.4

Table 1: Experimental ^{29}Si peak maxima and linewidth (full width at half max.) for β'-sialons (z = 1, 2, 4) along with associated errors and computational isotropic chemical shift (δ_{iso}) ranges for β'-sialon models.

The ^{27}Al MAS NMR spectra for the three samples show differences (e.g. linewidth, centre of the line) suggesting a change in the nature and/or relative proportions of the different local aluminium AlO_xN_{4-x} environments present with chemical composition (Figure 2, Table S3). However, the overlap caused by residual second-order quadrupolar broadening in the MAS NMR spectra means careful analysis is required to properly understand what the differences and underlying causes of them are. Two magnetic fields are used which then allows a better understanding of how the differing interactions (e.g., chemical shift, quadrupolar) contribute to the spectra, as has been widely used for ^{23}Na MAS NMR.[50] The peak positions and linewidth are summarised in Table S3. For each spectrum there are apparently sharper features, and care needs to be taken to distinguish these being caused by sites with small quadrupolar interactions and sharper features (e.g. singularities) of sites with larger quadrupolar interactions. One approach to improving the resolution of ^{27}Al MAS NMR spectra and getting an alternative perspective on the sites present is to employ 2D multiple-quantum (MQ) MAS techniques. Such ^{27}Al MQ MAS NMR spectra (Figure 3, also projections expanded in Figure S7) reveal some of the individual components that make up the 1D spectra, as well as highlighting significant overlap in the 1D spectra and the spread of sites present. For z = 1 the width in both dimensions of the plots indicate both a spread of chemically distinct sites and quite large quadrupolar interactions. It is important to note that if one looks at around δ_1 = 60 ppm although the signal to noise is quite poor, there is clearly intensity parallel to the Q-direction that spreads over a significant range, albeit somewhat ill-defined. Also, there is no noticeable intensity in the δ_2 range ~ 50 ppm which makes an interesting comparison with the z = 4 sample. In the 1D MAS NMR data as the linewidth decreases in ppm and remains roughly constant in Hz with increasing applied magnetic field confirms this interpretation as this is what one would expect with both quadrupolar and chemical shift dispersion contributing significantly to the observed linewidth.[50] In the MQ data it is clear that along the chemical shift (CS) direction the intensity does not extend to the AlO_4 region (i.e. (δ_1 = 40 ppm, δ_2 = 60 ppm)), suggesting that AlO_4 units only contribute weakly. Hence mixed AlO_xN_{4-x} ($1 \leq x \leq 3$) environments with significant quadrupolar interactions dominate.

For z = 2 the combination of 1D MAS, its field variation and 3Q MAS data shows a similar picture to z = 1, with again the spectrum dominated by sites with large quadrupolar interactions as indicated by the width parallel to the Q-direction, but with a wider range of

chemically different sites. The distribution however clearly shows a shift to lower ppm with a peak maximum in the 1D MAS at 75 ppm, indicating a greater proportion of local environments with more oxygen nearest neighbours. This is confirmed in the 3Q MAS data showing both a broad distribution, corresponding to mixed local aluminium environments, with the ridge extending towards lower chemical shifts, i.e., AlO_4 (Figure 3b) than for z = 1.

For z = 4 at higher ppm there is a very well-defined shoulder at 108 ppm (peak position). There is an additional peak(s) at 8 ppm, which corresponds to AlO_6. At this very high Al/O content, towards the high aluminium-content end limit for the formation of β'-sialon, it is likely due to some phase-separated impurities, as observed by XRD. XRD identifies the major secondary phase as ~10% 15R-polytypoid and is consistent with secondary phases identified in the formation of high z β'-sialons previously.[51] The positions of the observed peaks at 108 and 8 ppm are consistent with previous reports of the ^{27}Al MAS NMR spectrum of 15R-polytypoid and have been assigned to AlN_4 and AlO_6 respectively.[17] The presence of 15R-polytypoid has an impact on the composition of the remaining for β'-sialon portion, so that the actual z is a little below 4, which is estimated to be ~3.7. The rest of the observed signal lies between about 40 and 102 ppm, with a maximum at 78 ppm, and a shoulder to the left, corresponding to a range of mixed AlO_xN_{4-x} ($1 \leq x \leq 3$) environments, with the tail to the right corresponding to AlO_4. The ridge in the 3Q MAS data has become much more extended. The width of the ridge parallel to the Q-direction shows that there are some sites, which from their shift are likely to be mixed AlO_xN_{4-x} ($1 \leq x \leq 3$) units with significant quadrupolar interactions. However, when one gets into the region corresponding to AlO_4 (δ_1 ~ 35-40 ppm) the width parallel to the Q-direction is much reduced, indicating much smaller quadrupolar interactions for some of these sites. The field variation of the 1D MAS NMR spectra is also somewhat different from the z = 1 and z = 2 samples as it is almost constant in ppm suggesting that the linewidth is now more strongly dominated by chemical shift dispersion compared to the quadrupolar interaction. These observations about the ^{27}Al NMR data from the z = 4 sample are important for distinguishing the different models (vide infra).

Computational Methods

Two computational approaches were considered using DFT (CASTEP).[46] In the first approach the parent unit cell of β-Si_3N_4 (ICSD 8263) was used. Supercells were created to accommodate the different models, and Si/Al and N/O substitutions were made accordingly.

Prior to the calculation of NMR parameters, these model supercells were geometry optimised, both unit cell parameters and atomic coordinates, due to the substitutions. In the second approach the experimental unit cells for the substituted materials were used (ICSD 39496, 34288, 34287). Note that these crystal files contain unit cell parameters, and atomic coordinates, but with site occupancies averaged over the unit cell. That is, a particular site is defined with partial-occupancy of the two possible species Si/Al or N/O (for z = 1 a T-site is defined as occupied 83% by Si and 17% by Al). Therefore, they still required the creation of supercells and a distribution of Al/Si and O/N to cater for different models. The first approach was considered favourable as is it allowed unit cell expansion (due to differences in bond lengths etc.) without influence, which could then be compared to the changes observed in experimental unit cell parameters as the composition changes. Models (i) to (iv) as described in the introduction were examined. Further details of the models (i) to (iii) and the nomenclature used are given in the SI (Figure S2).

By simply allowing the respective sites within the β-Si_3N_4 structure to be populated randomly either by silicon/aluminium or oxygen/nitrogen the relative site intensities can be derived, with our analysis matching that in the supporting information of Ref. 18. For the z values studied here the relative intensities of the different AlO_xN_{4-x} coordinations are given in Table 2. The previous work of Cozzan *et al.*[18] clearly observed for low z values (z = 0.050, 0.075, and 0.125) that a stochastic model (i.e., random, statistical distribution) did not match the experimental ^{27}Al NMR data. Here this assertion can now be much more strongly constrained by the much wider range of z-values available. The random distribution has a significant proportion (p_n) (Table 2) of AlN_4 for z = 1 (59%) and z = 2 (32%), decreasing to ~ 6% for z = 4. Also at z = 4 the stochastic model predicts there to be very little AlO_4. These trends do not match what is observed experimentally, given the trends in where the intensity is observed relative to the expected shift (taking into account quadrupolar effects). Hence in agreement with previous measurements (e.g. NMR, X-ray spectroscopy) a random distribution can be immediately ruled out.

	z =1	z = 2	z = 4
Config.	**p_1 (%)**	**p_2 (%)**	**p_4 (%)**
AlN_4	58.6	31.6	6.2
$AlON_3$	33.5	42.2	25.0
AlO_2N_2	7.2	21.1	37.5
AlO_3N	0.7	4.7	25.0
AlO_4	0	0.4	6.2

Table 2. Distribution of AlO_xN_{4-x} units in different z-valued β'-sialons considering a random distribution of Si,Al and O,N over their respective sites.

Hence, the other three possible models of ordering (i) to (iii) are considered. The data on the crystal structures (Table S1, SI) provides the cell dimensions and volumes. The computational work allows the variation of the cell-related parameters with z to be calculated for each model. Then the NMR parameters from the corresponding local environments in each model can also be calculated and compared to the observed NMR spectra. From this approach it should be possible to conclude which model most closely describes what happens to the local atomic ordering in β'-sialons.

The experimental data on the crystal structure given in Table S1 provides the basis for the changes with composition. The fractional (%) changes in the a and c cell parameters, as well as the cell volume are given in Figure S8. The unit cell changes for the optimised structures from DFT calculations for the various models can be compared to the experimental data in Figure S9. All show the general trend of increasing lengths of cell edges and a corresponding increase in unit cell volume with increasing z, in agreement with what is observed experimentally. However strong differences in the variations of these parameters for each model with z can be seen. For the domain model there is no direct model constraint on the thickness of the domains, so two possible examples are taken as suggested in the original publication.[16] It can be seen (Figure S9 of the SI) that both the domain and channel models broadly reproduce the observed experimental variation in the cell parameters and volume, yet it appears to be very different for the plane model. Hence this observation strongly rules out the plane model from further consideration. The expansion of the unit cell observed experimentally is attributed to the difference in bond lengths (particularly, longer

Al-O compared to Si-N),[10] the distribution of which within the models influences the resulting unit cell parameters.

The NMR parameters calculated on the basis of the different structural models, can now be examined to distinguish the remaining two models ((i), (ii)), both of which have silicon mainly in SiN_4 environments, but with some mixed silicon environments. The DFT-calculated ^{29}Si isotropic chemical shifts for the β'-sialon models are shown in Figure 4. This shows a distribution of chemical shifts centred around a chemical shift of ~−48 ppm, but including a variety of local environments (SiN_4, SiN_3O, and SiO_2N_2). The figure shows at each z value the experimental data for the shift position and linewidth, and then above each the range of isotropic chemical shift values for the different local silicon environments in variants of the different models (Figures 1, S2). Calculations show that a range of local coordinations i.e. SiO_xN_{4-x} are covered by the experimental linewidths observed. These new calculations show that for all of the silicon environments present, the isotropic chemical shifts (δ_{iso}) do not show large changes in these materials, such that simply equating the observed chemical shift at around −48 ppm as 'proving' only an SiN_4 environment[35-37] is a little too simplistic. It is known that as well as the effect of the nearest neighbour on δ_{iso} there are the effects of local geometry (e.g., bond lengths and bond angles)[26,27] which means different contributions to δ_{iso} can lead to strong overlap of the SiN_4 and SiN_3O environments. The observed ^{29}Si experimental peak positions and linewidths cover all the local environments in each of the models (see Fig. 4), apart from an outlier SiO_2N_2 associated with the plane 221 model for z = 2. However, the intensity of this site would be very low and difficult to detect. The plane model does not show a good match of the spread of chemical shifts of the environments to the changes of observed linewidth (Table 2). For example, the calculations show in the plane model a much reduced range of shifts for z = 4 compared to z = 2, which is opposite to the trend in the experimental linewidth. This underlines that the plane model should be discounted, as suggested above on the basis of the observed cell parameter variation. On the basis of the ^{29}Si MAS NMR data models (i) and (ii) cannot be distinguished.

The situation for interpreting ^{27}Al NMR data is more complex as there are both chemical shift and quadrupolar interactions (δ_{iso}, quadrupolar parameters C_Q and η_Q).[26,28,31] The possible local environments of aluminium within a defect-free structure are: AlO_4, AlO_3N, AlO_2N_2, $AlON_3$ and AlN_4. There are two structurally-distinct nitrogen sites (N^1, N^2) in the parent structure. Each aluminium is surrounded by four such sites, three of type N^1 and one of type

N^2. Hence given these are structurally-distinct sites the local aluminium environments can be further described by how the oxygen and nitrogen are distributed across these two sites (N^1, N^2) in the mixed environments, i.e., $AlO_3^{112}N^1$, $AlO_3^{111}N^2$, $AlO_2^{12}N_2^{11}$, $AlO_2^{11}N_2^{12}$, $AlO^2N_3^{111}$, and $AlO^1N_3^{112}$. The NMR parameters (δ_{iso}, C_Q) for the different local environments extracted from the models are summarised in Figure 5. This shows a range of parameters for the different environments. The larger C_Qs (as observed experimentally in the MQMAS spectra and calculated for the models) for the mixed environments AlO_xN_{4-x} creates significant overlap in the 1D MAS NMR spectra, and comprise most of the signal seen in them. The one AlN_4 also has quite a large C_Q which at first sight may be quite surprising in comparison to the previous calculations[18], but here it is at high z, so is more structurally constrained here (Figure S10). As a check we used our DFT approach to calculate the ^{27}Al NMR parameters for z = 0.125 β'-sialon. There is close agreement of the calculated quadrupolar parameters for the different local coordinations at this composition between this study and the values reported in Ref. 18 (Figure S11). Also to make it clearer which sites are associated with which model, the calculated δ_{iso} and C_Q associated with the sites from each model is individually shown (Figure 5(b) for z = 4 and S12 for the domain and channel models).

Distinguishing the Domain and Channel Models

The observations above have clearly ruled out the random (iv) and plane models (iii) which will not be considered further here. In considering the ^{29}Si MAS NMR data some of the channel models do not give a good match with the ^{29}Si shift ranges, with ^{29}Si data from the domain models giving a better match. However, this distinction is not sufficiently definitive to be categorical as to which model is correct. We believe that the ^{27}Al NMR data is definitive when comparing the complete set of information available here. The channel model only contains one Al local coordination (AlO_3N). This arises as the 'channels' are solely comprised of Al and O, with the Al bonding to the rest of the framework via N. There is also only one Si local environment, SiN_4, although in both cases there is variation in next-nearest neighbours. The reason the channel model can be ruled out is these mixed aluminium environments AlO_3N *only* produce sites with large C_Q (Figure 5b, Figure S12 bottom). The domain model has a variety of local aluminium environments. Although the relative intensity of these depend on the relative thickness of the aluminium-containing to silicon-containing layers, *all* thicknesses show a mixture of environments with more oxygen-rich environments with significantly

smaller C_Qs. The extension of the ridge in the 3Q MAS NMR data is down to a region more associated with AlO_4 for the z = 4 sample. What is really important in this figure is the shift of coordinates where intensity (δ_1, δ_2) appears and changes with z, and if one moves along the CS direction the changes of the extent parallel to the Q-direction at each point. It is very clear, although noisy, the extent parallel to Q decreases very significantly at (~40 ppm, ~50 ppm) compared to say (~60 ppm, ~100 ppm) for z = 4. This means there *must* be both large and small C_Qs sites present. The calculations of the NMR parameters (Figure S12) show the channel model only has sites with large C_Qs whereas the domain model has a wide range. Hence the channel model is not consistent with this experimental observation. To reinforce this point of distinction the positions on the 3Q data sets where the coordination units in the model would produce intensity are shown as red diamonds superimposed on the MQ data sets (Figure S13). It is clearly seen that the calculated positions for the channel model do not cover a wide enough range of positions, while the domain model is a much better match. Hence it is particularly clear by considering both the match of the spread of intensity in the 3Q data *and* the absence of sites with smaller C_Qs in the channel model that means this model can be strongly ruled out. This only leaves the domain model as being consistent with all of the data *viz.* the changing cell parameter and cell volume, along with the NMR information about the range and nature of the local environments, combined with the DFT-calculated values compared with the observations.

Much more speculatively one could now potentially 'invert' the data. That is to say, taking the domain model as a starting point, then one can compare the calculated ^{27}Al MAS NMR spectra with different layer thicknesses to potentially estimate that layer thickness. Figures S14 shows the experimental spectra recorded at 20.0 T, and spectra simulated using SIMPSON.[52] The simulated spectra use the calculated NMR parameters for the domain models. From a purely visual comparison, the models that give the best match are: for z = 1 the domain 116 model and for z = 2 the domain 113 model; these both equate to a single layer thickness of Al substitution, where a layer is defined by a unit cell of the parent structure (Figure S3). However, some thicker regions (e.g., double layer) are also expected for z = 2 to accommodate the AlO_4 units observed in the experimental MQMAS spectra. Simulated ^{27}Al MAS NMR spectra for the other models and fields are given in the SI (Figures S15-17). Support for the domain model is given by the ^{29}Si NMR data, where the computed isotropic chemical shift ranges give a good match to the experimental linewidth (Table 1, Figure 4), particularly

for z = 1 (expt. 2.3 ppm, domain 116 model 2.5 ppm). Then for z = 2 the calculation show an increase in linewidth which is observed experimentally. For z = 4 the impurities/defects preclude such a comparison.

Conclusions

Previous observations of the ^{27}Al MAS NMR spectra from aluminium-dilute β'-sialons (z = 0.050, 0.075, and 0.125), have been considerably extended here to very much higher z (z = 1-4) to constrain the local ordering and distinguish between the different structural models that have been proposed. This study used literature values of the variation of the cell-related parameters and the ^{29}Si and ^{27}Al MAS NMR data, to quantify the changes in the structure and local environments of these nuclei. The key here using DFT calculations of *both* the structure and NMR parameters that allowed the four competing models to be distinguished by comparison of the experimental variation with the calculated values as the composition is varied. Only one, the original NMR domain model is fully consistent with all of the data recorded. This is the first time for β'-sialons that such a detailed picture of the structure has been possible, which will be important for the developing applications of these materials. It may also be possible to constrain the model further by describing the thickness of the layers, through a comparison of simulated and experimental ^{27}Al MAS NMR spectra.

Supporting Information

Structural parameters and model structure, summary of previous NMR reports from β'-sialons, reference shielding for DFT (CASTEP) calculations, ^{29}Si MAS NMR data, ^{27}Al MAS NMR data, experimental and calculated variations in the unit cell parameters and various calculations of the ^{27}Al NMR data based on the local environments predicted by the different structural models, example SIMPSON input files.

Acknowledgments

Lancaster University is thanked for provision of the NMR, XRD and HEC facilities, and for funding this research. Characterisation facilities were part funded by the European Regional Development Fund (ERDF) under the collaborative Technology Access Program (cTAP). Dr Nathan Halcovitch (Lancaster University) is gratefully acknowledged for providing XRD support. The UK 850 MHz solid-state NMR Facility used in this research was funded by

EPSRC and BBSRC (contract reference PR140003), as well as the University of Warwick including via part funding through Birmingham Science City Advanced Materials Projects 1 and 2 supported by Advantage West Midlands (AWM) and the European Regional Development Fund (ERDF). Collaborative assistance from the 850 MHz Facility Manager (Dinu Iuga, University of Warwick) is acknowledged.

References

(1) Jack, K.H. Wilson W.I. Ceramics based on Si-Al-O-N systems. *Nature* **1972**, *238*, 28-29.
(2) Jack, K.H. Sialons and related ceramics. *J. Mater. Sci.* **1976**, *11*, 1135-1158.
(3) Gauckler, L.J.; Lukas, H.L.; Petzow, G. Contribution to phase diagram Si_3N_4-AlN-Al_2O_3-SiO_2. *J. Amer. Ceram. Soc.* **1975**, *58*, 346-347.
(4) Grün R. Crystal-structure of β-Si_3N_4 – structure and stability considerations between α-Si_3N_4 and β- Si_3N_4. *Acta Crystallogr. B* **1979**, *35*, 800-804.(5) Ekstrom, T.; Nygren M. Sialon ceramics. *J. Amer. Ceram. Soc.* **1992**, *75*, 259-276.
(6) Gillott, L.; Cowlam, N.; Bacon, G.E. A neutron-diffraction investigation of some β'-sialons. *J. Mater. Sci.* **1981**, *6*, 2263-2268.
(7) Hirosaki, N.; Xie, R.J.; Kimoto, K.; Sekiguchi, T.; Yamamoto, Y.; Suehiro, T.; Mitomo, M. Characterization and properties of green-emitting β-SiAlON: Eu^{2+} powder phosphors for white light-emitting diodes. *Appl. Phys. Lett.* **2005**, *86*, 211905.
(8) Kimoto, K., Xie, R.J., Matsui, Y., Ishizuka, K., Hirosaki, N., Direct observation of single dopant atom in light-emitting phosphor of β-SiAlON:Eu^{2+}. *Appl. Phys. Lett.* **2009**, *94*, 041908.
(9) Cozzan, C.; Laurita, G.; Gaullois, M.W.; Cohen, M.; Mikhailovsky, A.A.; Balasubramanian, M.; Seshadri, R. Understanding the links between composition, polyhedral distortion, and luminescence properties in green-emitting β-$Si_{6-z}Al_zO_zN_{8-z}$:Eu^{2+} phosphors. *J. Mater. Chem. C* **2017**, *5*, 10039-10046.
(10) Merkx, E.P.J.; van Overbeek, S., van der Kolk, E. Functionalizing window coatings with luminescence centers by combinatorial sputtering of scatter-free amorphous SiAlON:Eu^{2+} thin film composition libraries. *J. Luminesc.* **2019**, *208*, 51-56.
(11) van Dijen, F.K.; Metselaar, R.; Helmholdt, R.B. Neutron diffraction study of β'-sialon. *J. Mater. Sci. Lett.* **1987**, *6*, 1101-1102.
(12) Khatinskaya, D.Y.; Em, V.T.; Loryan, V.E.; Smirnov, K.L. A neutron diffraction study on the structure of β'-sialon. *Inorg. Mater.* **1991**, *27*, 1805-1807.
(13) Sjöberg, J.; Ericsson, T.; Lindqvist, O. Local-structure of β'-sialons – An EXAFS study. *J. Mater. Sci.* **1992**, *27*, 5911-5915.
(14) Hagio, T.; Takase, A.; Umebayashi, S. X-ray photoelectron spectroscopic studies of β-sialons. *J. Mater. Sci. Lett.* **1992**, *11*, 878-880.
(15) Tatsumi, K.; Mizoguchi, T.; Yoshioka, S.; Yamamoto, T.; Suga, T.; Sekine, T.; Tanaka, I. Distribution of solute atoms in β- and spinel $Si_{6-z}Al_zO_zN_{8-z}$ by AlK-edge X-ray absorption near-edge structure. *Phys. Rev. B* **2005**, *71*, 033202.
(16) Dupree, R.; Lewis M.H.; Smith, M.E. Structural characterization of ceramic phases with high-resolution ^{27}Al NMR. *J. Appl. Cryst*. **1988**, *21*, 109-116.
(17) Smith, M.E. Observation of mixed $Al(O,N)_4$ structural units by ^{27}Al magic angle spinning NMR. *J. Phys. Chem.* **1992**, *96*, 1444-1448.

(18) Cozzan, C.; Griffith, K.J.; Laurita, G.; Hu, J.G.; Grey, C.P.; Seshadri, R. Structural Evolution and Atom Clustering in β-SiAlON: β-$Si_{6-z}Al_zO_zN_{8-z}$ *Inorg. Chem*. **2017**, *56*, 2153-2158.
(19) Okatov, S.V.; Ivanovskii, A.L. Chemical bonding and atomic ordering effects in β′-sialon. *Int. J. Inorg. Mater.* **2001**, *3*, 923-930.
(20) Okatov, S.V.; Shveikin, G.P.; Ivanovskii, A.L. Modelling of atomic ordering effects in multicomponent systems: sialons and sibeons. *Dokl. Phys. Chem.* **2003**, *388*, 38-41.
(21) Tatsumi, K.; Tanaka, I.; Adachi, H.; Yoshiya, M. Atomic structures and bondings of β- and spinel $Si_{6-z}Al_zO_zN_{8-z}$ by first principles calculations. *Phys. Rev. B*, **2002**, *66*, 165210.
(22) Momma K.; Izumi, F. VESTA 3 for three-dimensional visualization of crystal, volumetric and morphology data. *J. Appl. Crystallogr.* **2011**, *44*, 1272-1276
(23) Fang, C.M.; Metselaar, R. Site preferences in β-sialon from first-principles calculations. *J. Mater. Chem.* **2003**, *13*, 335-337.
(24) Fang, C.M.; Metselaar, R. First-principles calculations of microdomain models for β-sialon Si_5ALON_7. *J. Amer. Ceram. Soc.* **2003**, *86*, 1956-1958.
(25) Boyko, T.D.; Gross, T.; Schwarz, M.; Fuess, H.; Moewes, A. The local crystal structure and electronic band gap of β-sialons. *J. Mater. Sci.* **2014**, *39*, 3242-3252.
(26) MacKenzie, K.J.D.; Smith, M.E. *Multinuclear Solid State NMR of Inorganic Materials*, Pergamon, 2002.
(27) Engelhardt G.; Michel, D. *High Resolution Solid State NMR of Silicates and Zeolites*. John Wiley & Sons, 1987.
(28) Smith, M.E. Applications of ^{27}Al NMR techniques to structure determination in solids. *Appl. Magn. Reson.* **1993**, *4*, 1-64.
(29) Eden, M. ^{27}Al NMR studies of aluminosilicate glasses. *Ann. Rep. NMR Spectrosc.* **2015**, *86*, 237-331.
(30) Hauoas, M.; Taulelle, F.; Martineau, C. Recent advances in application of ^{27}Al NMR spectroscopy to materials science. *Prog. NMR Spectrosc.* **2016**, *94-95*, 11-36.
(31) Smith, M.E.; van Eck, E.R.H. Recent advances in experimental solid state NMR methodology for half-integer spin quadrupolar nuclei. *Prog. NMR Spectrosc.* **1999**, *34*, 159-201.
(32) Smith M.E. *in Solid-state NMR spectroscopy of inorganic materials*, Ed. Fitzgerald, J.J., *ACS Symposium Series* **1998**, *717*, 377-404.
(33) Dupree, R.; Lewis, M.H.; Smith, M.E. High-resolution ^{29}Si nuclear magnetic resonance in the Y-Si-O-N system. *J. Am. Chem. Soc.* **1988**, *110*, 1083-1087.
(34) Dupree, R.; Lewis, M.H.; Smith, M.E. A high-resolution NMR-study of the La-Si-Al-O-N system. *J. Am. Chem. Soc.* **1989**, *111*, 5125-5132.
(35) Dupree, R.; Lewis, M.H.; Leng-Ward, G.; Williams, D.S. Coordination of Si atoms in silicon-oxynitrides determined by magic-angle-spinning NMR. *J. Mater. Sci. Lett.* **1985**, *4*, 393-395.
(36) Carduner, K.R.; Carter, R.O.; Millberg M.E.; Crosbie, G.M. Determination of phase-composition of silicon-nitride powders by ^{29}Si magic angle spinning nuclear-magnetic-resonance spectroscopy. *Anal. Chem.* **1987**, *59*, 2794-2797.
(37) Carduner, K.R.; Blackwell, C.S.; Hammond, W.B.; Reidinger, F.; Hatfield, G.R. ^{29}Si NMR characterization of α-silicon and β-silicon nitride. *J. Am. Chem. Soc.* **1990**, *112*, 4676-4679.
(38) Harris, R.K.; Leach, M.J.; Thompson D.P. Synthesis and magic-angle spinning nuclear magnetic resonance of ^{15}N-enriched silicon nitrides. *Chem. Mater.* **1990**, *3*, 320-323.
(39) Sjöberg, J.; Harris R.K.; Apperley D.C. ^{29}Si, ^{27}Al and ^{15}N magic-angle spinning nuclear magnetic resonance of O′-sialons and some related phases. *J. Mater. Chem.* **1992**, *2*, 433-438.

(40) Hanna, J.V.; Smith, M.E. Recent technique developments and applications of solid state NMR in characterising inorganic materials. *Solid State Nucl. Magn. Reson.* **2010**, *38*, 1-18.
(41) Medek, A.; Harwood, J.S.; Frydman, L. Multiple-quantum magic-angle spinning NMR: A new method for the study of quadrupolar nuclei in solids. *J. Am. Chem. Soc.* **1995**, *117*, 12779-12787.
(42) Brown, S.P.; Wimperis, S. Two-dimensional multiple-quantum MAS NMR of quadrupolar nuclei: A comparison of methods. *J. Magn. Reson.* **1997**, *128*, 42-61.
(43) Gan, Z.; Kwak, H.T. Enhancing MQMAS sensitivity using signals from multiple coherence transfer pathways. *J. Magn. Reson.* **2004**, *168*, 346-351.
(44) Ball, T.J.; Wimperis, S. Use of SPAM and FAM pulses in high-resolution MAS NMR spectroscopy of quadrupolar nuclei. *J. Magn. Reson.*, **2007**, *187*, 343-351.
(45) Pike, K.J.; Malde, R.P.; Ashbrook, S.E.; McManus, J.; Wimperis, S. Multiple-quantum MAS NMR of quadrupolar nuclei. Do five-, seven- and nine-quantum experiments yield higher resolution than the three-quantum experiment? *Solid State Nucl. Magn. Reson.* **2000**, *16*, 203-215.
(46) Clark, S.J.; Segall, M.D.; Pickard, C.J.; Hasnip, P.J.; Probert, M.J.; Refson, K.; Payne, M.C. First principles methods using CASTEP. *Zeit. Kristall.* **2005**, *220*, 567-570.
(47) Pickard, C.J., Mauri, F., All-electron magnetic response with pseudopotentials: NMR chemical shifts. *Phys. Rev. B*, **2001**, *63*, 245101.
(48) Yates, J.R.; Pickard, C.J.; Mauri, F. Calculation of NMR chemical shifts for extended systems using ultrasoft pseudopotentials. *Phys. Rev. B* **2007**, *76*, 024401.
(49) Profeta, M.; Mauri, F.; Pickard, C.J. Accurate first principles prediction of ^{17}O NMR parameters in SiO_2: Assignment of the zeolite ferrierite spectrum. *J. Am. Chem. Soc.* **2003**, *125*, 541-548.
(50) Kohn, S.C.; Dupree, R.; Smith, M.E. A multinuclear magnetic-resonance study of the structure of hydrous albite glasses. *Geochim. Cosmochim. Acta*, **1989**, *53*, 2925-2935.
(51) MacKenzie, K.J.D.; Meinhold, R.H. Additive-assisted pressureless sintering of carbothermal β'-sialon: an X-ray and solid-state MAS NMR study. *J. Mater. Chem.* **1996**, *6*, 821-831.
(52) Bak, J.M.; Rasmussen J.T.; Nielsen, N.C. SIMPSON: A general simulation program for solid-state NMR spectroscopy. *J. Magn. Reson.*, **2000**, *147*, 269-330.

Figures

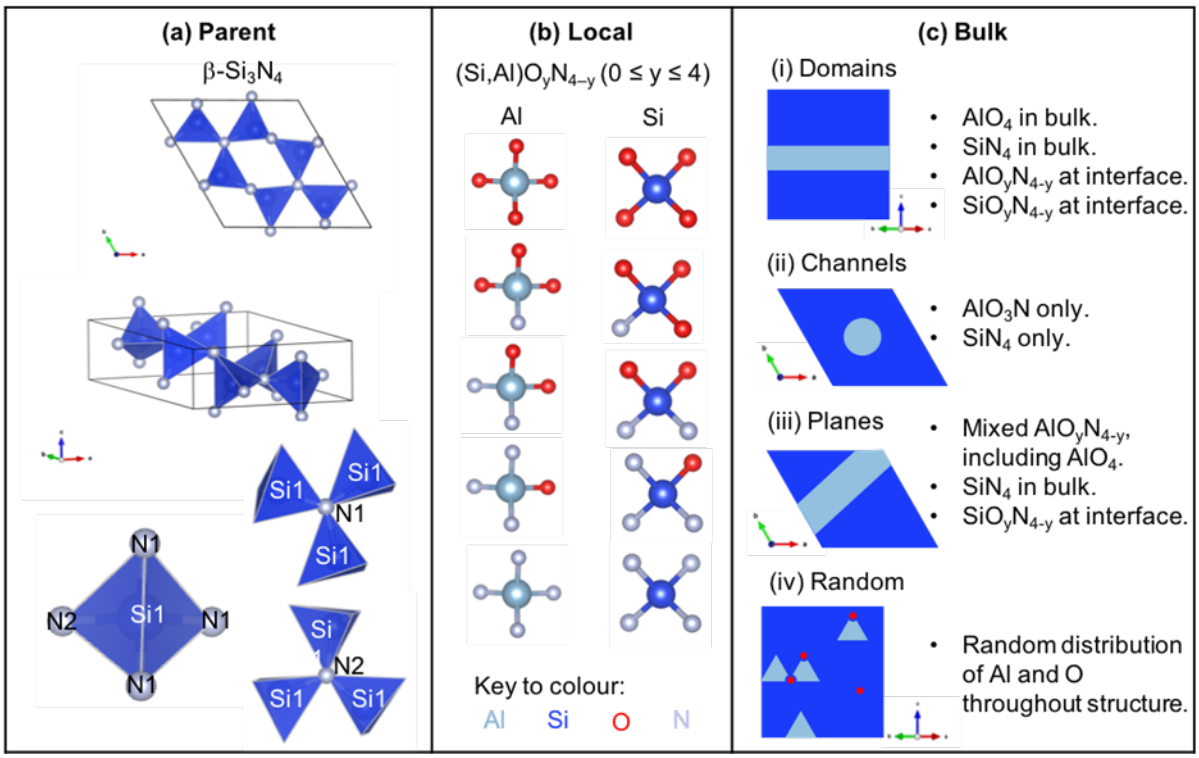

Figure 1: Structure of (a) β-Si_3N_4 showing the three crystallographically-distinct sites, (b) the possible local coordination units around the silicon and aluminium in β'-sialons and (c) schematic representations of different proposed structures of β'-sialons. Unit cell and local environment figures were created using VESTA.[22]

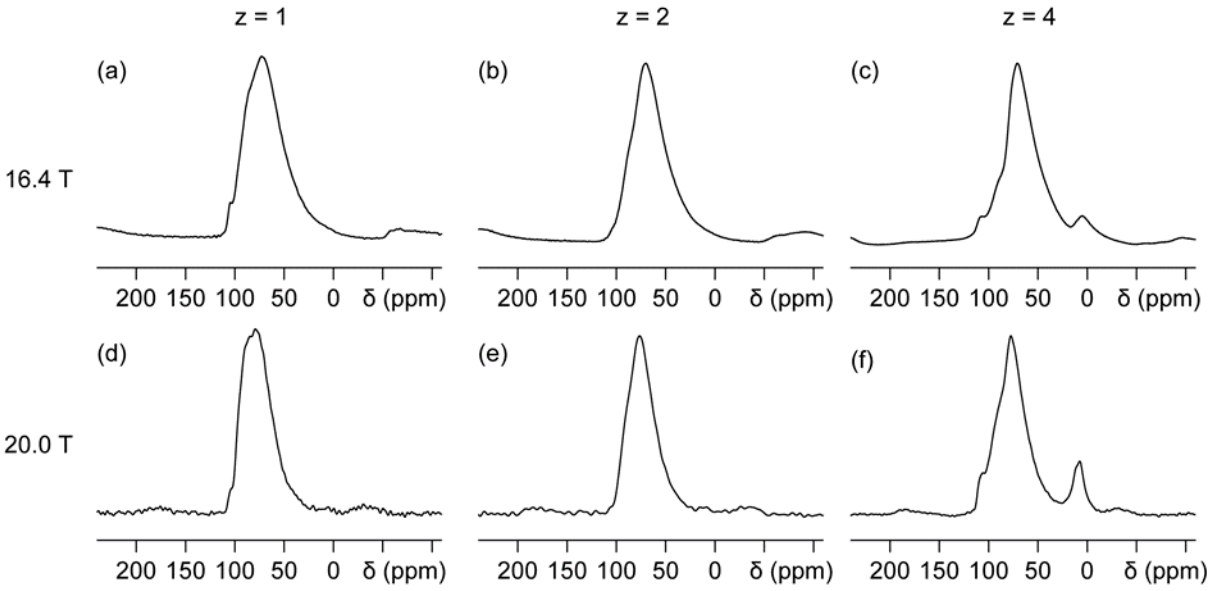

Figure 2: ^{27}Al MAS NMR spectra (16.4 T, 30 kHz MAS; 20.0T, 25 kHz MAS) for (a,d) z = 1, (b,e) z = 2, (c,f) z = 4.

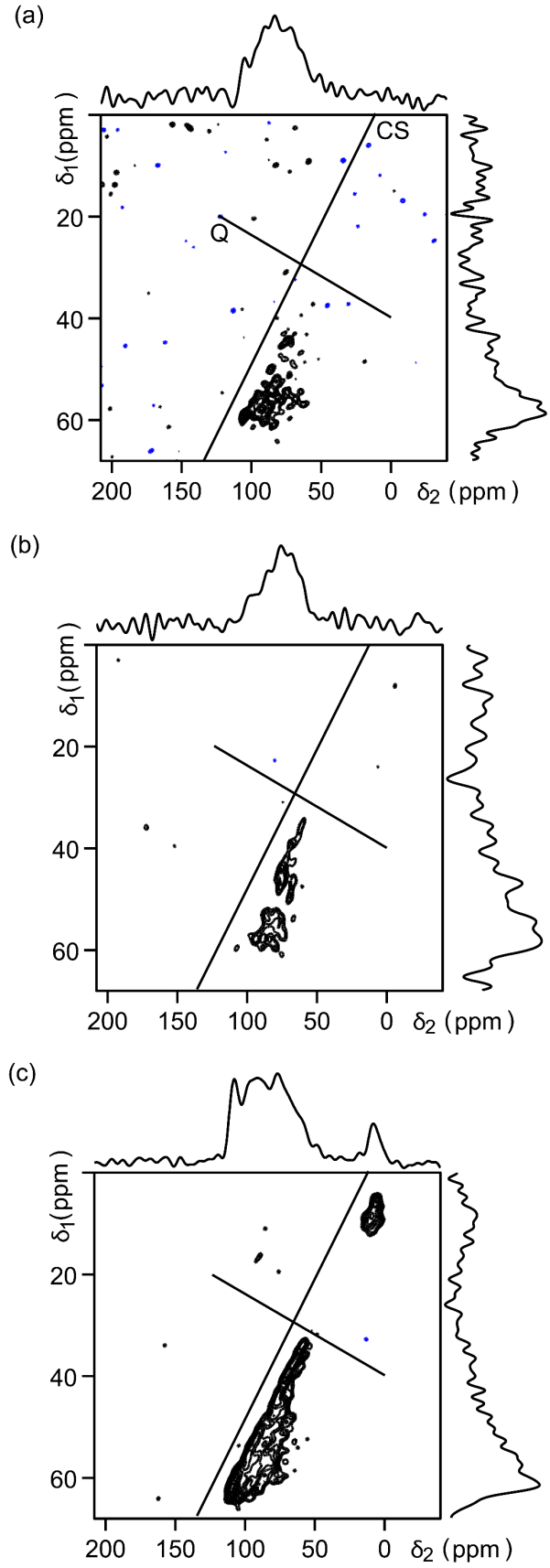

Figure 3: ^{27}Al MQMAS NMR spectra (20.0 T, 25 kHz MAS), for (a) z = 1, (b) z = 2, and (c) z = 4. Solid lines indicate directions of dispersion for chemical shift (CS) and second-order quadrupolar (Q) interactions. The projections onto the δ_1 and δ_2 axes are shown.

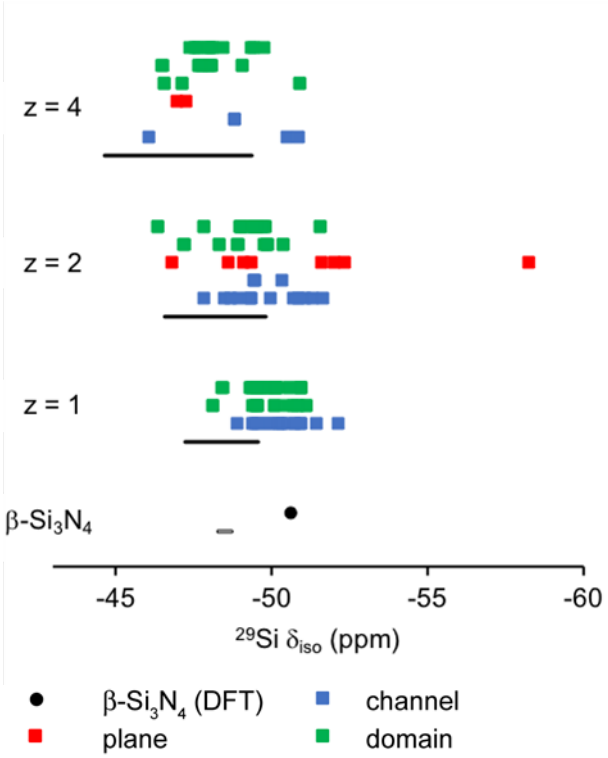

Figure 4: Calculated ^{29}Si isotropic chemical shifts (δ_{iso}). Dots β-Si_3N_4 black line experimental δ_{iso}), Squares β'-sialons (blue for channels, red for planes, green for domains). The solid black lines indicate the experimental full width at half maximum, which is seen experimentally to increase with z, and are centred around the individually observed experimental peak maxima. The outlier is from a SiO_2N_2 local environment from the plane 221 model for z = 2.

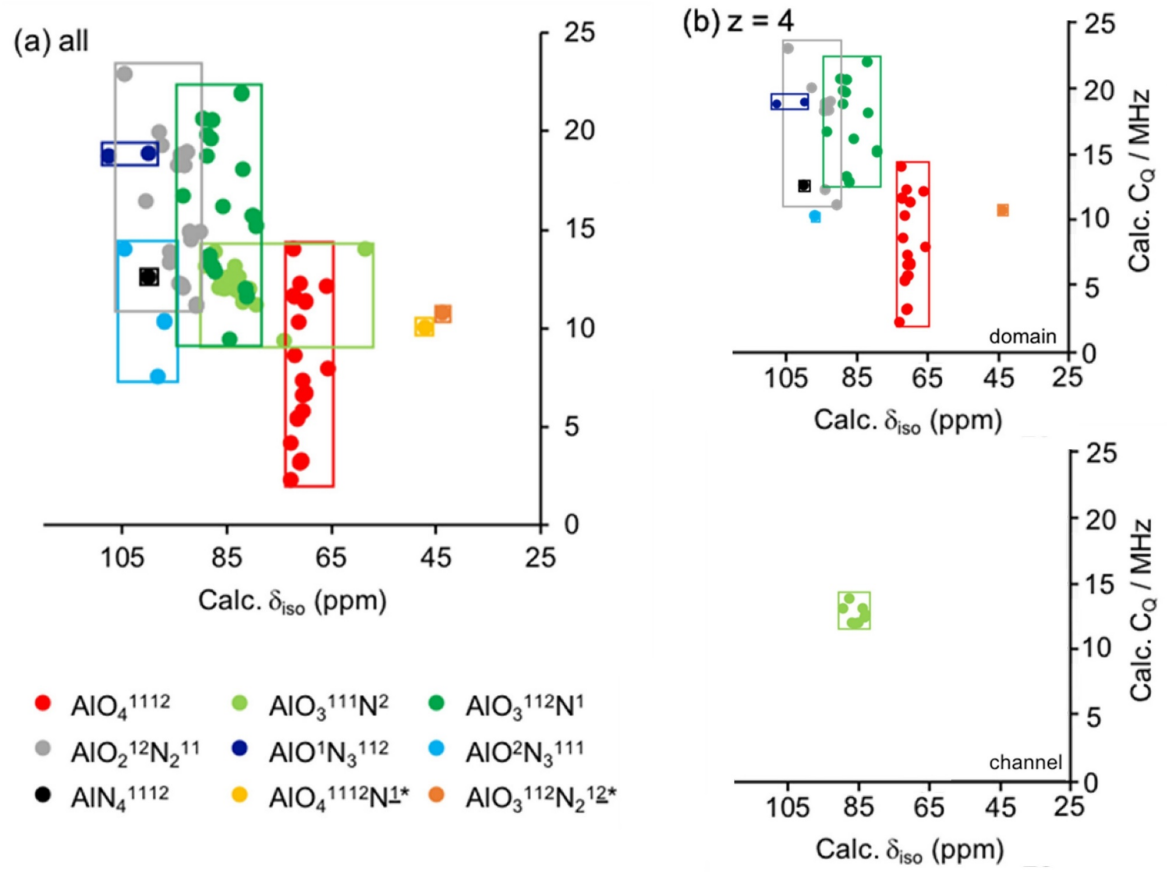

Figure 5: Plot of calculated (CASTEP) ^{27}Al NMR parameters*for* (a) all the models and (b) z = 4 domain (top) and channel (bottom) models; isotropic chemical shift (δ_{iso}) and quadrupolar coupling (C_Q). The * outliers are from defects found in models plane 221 and domain 116ii for z = 4, the outlier in the $AlO_3^{111}N^2$ category is also from the plane 221 model.

For Table of Contents Only